

Unsupervised Multi-modal Feature Alignment for Time Series Representation Learning

Chen Liang

Harbin Institute of Technology
Harbin, China
23B903050@stu.hit.edu.cn

Donghua Yang

Harbin Institute of Technology
Harbin, China
yang.dh@hit.edu.cn

Zhiyu Liang

Harbin Institute of Technology
Harbin, China
zyliang@hit.edu.cn

Hongzhi Wang

Harbin Institute of Technology
Harbin, China
wangzh@hit.edu.cn

Zheng Liang

Harbin Institute of Technology
Harbin, China
lz20@hit.edu.cn

Xiyang Zhang

Harbin Institute of Technology
Harbin, China
7203610125@stu.hit.edu.cn

Jianfeng Huang

Harbin Institute of Technology
Harbin, China
JFHuang.research@gmail.com

Abstract—In recent times, the field of unsupervised representation learning (URL) for time series data has garnered significant interest due to its remarkable adaptability across diverse downstream applications. Unsupervised learning goals differ from downstream tasks, making it tricky to ensure downstream task utility by focusing only on temporal feature characterization. Researchers have proposed multiple transformations to extract discriminative patterns implied in informative time series, trying to fill the gap. Despite the introduction of a variety of feature engineering techniques, e.g. spectral domain, wavelet transformed features, features in image form and symbolic features etc. the utilization of intricate feature fusion methods and dependence on heterogeneous features during inference hampers the scalability of the solutions. To address this, our study introduces an innovative approach that focuses on aligning and binding time series representations encoded from different modalities, inspired by spectral graph theory, thereby guiding the neural encoder to uncover latent pattern associations among these multi-modal features. In contrast to conventional methods that fuse features from multiple modalities, our proposed approach simplifies the neural architecture by retaining a single time series encoder, consequently leading to preserved scalability. We further demonstrate and prove mechanisms for the encoder to maintain better inductive bias. In our experimental evaluation, we validated the proposed method on a diverse set of time series datasets from various domains. Our approach outperforms existing state-of-the-art URL methods across diverse downstream tasks. Experiments confirm its enhanced representation power and superior scalability due to its model-agnostic nature. Additionally, this paper introduces a novel paradigm for time series URL through multi-modal feature alignment, paving a new research direction in this domain.

Index Terms—Unsupervised representation learning, Multivariate time series, Feature engineering, Feature alignment, Spectral graph theory, Inductive bias

I. INTRODUCTION

Time series describes a variable over time and encompasses various measures of monitoring of an entity such as an organism’s electrical signals and the CPU usage of a system or device. Multivariate time series (MTS) involves sets of dependent variables, playing a pivotal role across domains from finance to healthcare and the natural sciences [1]–[4].

Despite accumulating extensive time series data from various fields, understanding patterns within time series still remains challenging, even for domain experts. In contrast to images and text, where certain patterns are quickly discernible, time series pose complexities in pattern identification and analysis. This feature further increases the difficulty of obtaining labels for supervised learning [5]. Thus, unsupervised representation learning (URL) for time series [6]–[9] has thus emerged as a recent research focus. *URL aims to train a neural network (called encoder), without requiring labels, to encode the data into feature vectors (feature or embedding), by using subtly designed supervision signals to capture semantic equivalence by leveraging inherent patterns of the raw data.* The learned representation, necessitating minimal annotation [10], proves valuable in a variety of downstream tasks like temporal data classification, clustering, anomaly detection [8], [9], retrieval [11], etc.

From the aspect of complexities of mixed discriminative and irrelevant patterns, time series pose challenges for representation learning. Time series data can be blended with blind-source noise, acquired through varied methods, and exhibit intricate distributions and semantics [12]. Even though various feature engineering methods are proposed to parse time series and expose abundant discriminative patterns that are more tangible to observe, the complex and diversiform nature of time series engineering methods decrease their applicability for time series URL [5], [6] preventing the encoders from avoiding misinterpretation of patterns and gaining generalization ability by learning from diverse multi-modal features.

More specifically, variety of feature engineering methods and heterogeneity of the multi-modal features of time series data make the utilization of the features intricate [7], [13]–[15].

On one hand, most of the feature engineering methods for time series are highly coupled with neural structure of the encoder, making it difficult to design a scalable encoder to encode all kinds of feature obtained. During inference, time consumption for such feature acquirement is also inevitable,

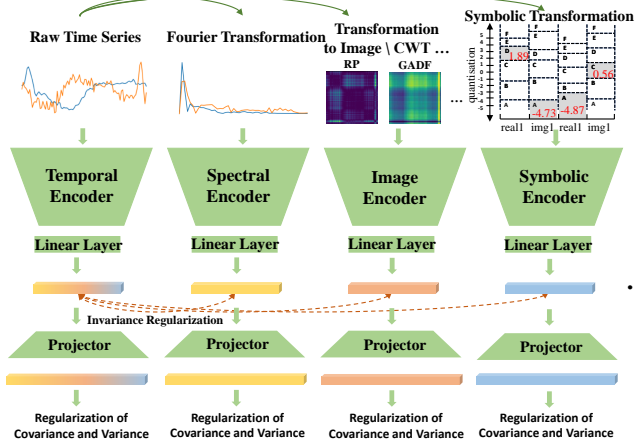


Fig. 1. **An overview of the MMFA framework.** A range of transformations is applied to raw time series data to produce discriminative features across multiple modalities. These features are subsequently processed by asymmetric neural feature extractors to uncover significant patterns. Following this, the representations are mapped to a common semantic space and brought into alignment through the use of regularization techniques. The framework readily accommodates various combinations of transformations and encoders, facilitating improved performance and adaptability to diverse problem setups.

overly complicated neural architecture can also hurt the overall performability. For example, [7] propose a dual tower structure to fuse time and spectral domain features, filling the inductive gap (i.e. learning from different patterns) between these two views. Nevertheless, researchers have explored transforming time series data into image [14], [15] or symbol sequences [13], [16] to comprehend them better. While feature fusion allows learning from multiple modalities, it often requires intricate multi-tower neural architectures tailored to handle specific feature attributes [7], [13], [15]. However, the adoption of such structures may overly complicate the neural network, warranting consideration. Moreover, the complexities inherent in feature engineering can significantly increase the computational cost, potentially elevating the overall inference complexity.

On the other hand, various transformations for feature engineering captures patterns from different perspective, leading to inductive gaps between neural learners trained from different features [7]. Learning from each of the transformed features respectively fail to fill the gap. Besides, when fusing knowledge learned from the features together, the encoder merely needs to identify easily learnable patterns [17], without considering semantic equivalence between different discriminative patterns extracted from multi-modal features, which causes information loss, misinterpretation of data and decreased model performance.

To fill the gap caused by intrinsic feature engineering for time series URL and the absence of technique that can leverage the abundant patterns, we pursue a model-agnostic framework for injecting knowledge about various patterns implied in multi-modal features to the raw time series encoder. This encoder essentially recovers significant elements of inductive

bias, i.e., the knowledge that makes the algorithm learn from one pattern instead of another pattern, acquired through various transformations and feature extraction processes. To capture equivalent patterns of each of the modalities, we construct graphs that depict semantic similarities of the feature entities. The alignment of such graphs naturally creates a supergraph, on which encoders are enhanced by placing a stronger emphasis on and facilitating the distribution matching of crucial patterns lies in multi-modal features.

Since the alignment of the subgraphs fine-tunes the connectivity of the subgraph corresponded to raw time series modality by connecting it to the other subgraphs, preserving the neural encoder for the temporal domain is adequate during URL inference. Thus, while ensuring high utility, we achieve greater scalability than traditional feature fusion approaches. To the best of our knowledge, we are the first who explore feature alignment for time series. Our analysis demonstrate textcoloreda notable advantage of our proposed framework compared to single-modal methods.

Furthermore, to learn equivalent multi-modal patterns from the graph, we propose regularization methods that treat the unsupervised learner as a spectral embedding learner on the graph. In practice, we leverage combinations of discriminative transformations and neural feature encoders to reconstruct the super-graph using distances between the output representations. During the train phase of the designed regularization terms, the encoders gradually adapts to fit the eigenfunctions of the graph laplacian operator of the super-graph with small eigenvalues. Such that we divide both the super-graph and subgraphs into more meaningful clusters and infuses the knowledge introduced by transformations into the encoder. Thus, the positive and negative sample pairs construction to mimic the unknown distribution of the original equivalence relations between them is eliminated. As a result, our multi-modal feature alignment framework (MMFA) outperforms existing state-of-the-art approaches.

The main contributions of this paper are summarized as follows:

- We introduce a novel feature-aligned URL framework, enhancing the utility of URL while maintaining scalability, demonstrate and theoretically analyse the key mechanisms of it.
- We eliminate of mimicking unknown distributions by constructing semantic equivalence graph of multi-modal features, and fitting encoders to the eigenfunctions of the super-graph, resulting in superior performance compared to state-of-the-art approaches for MTS URL tasks.
- Through experiments on time data tasks in different domains, we find that i) the time series representation learned by our method can achieve the highest performance on multiple downstream tasks, such as classification, clustering, and anomaly detection; ii) Our proposed approach outperforms all existing URL approaches by a large margin, comparable (or even better than) approaches tailored to downstream tasks.

- We propose a time series URL paradigm based on alignment and regularization, pointing toward a new URL research direction. Shine light on a new way towards more unified URL methods for multivariate time series for the researchers.

II. RELATED WORK

In this section, we provide an overview of the research in the landscape within the domain of our work. We categorize the related work into three themes and discuss their contributions, limitations, and relevance to our work.

A. URL for MTS

URL on time series data has emerged as a powerful approach eliminating the need for human supervision in obtaining meaningful representations [18]. Deep learning techniques such as autoencoders and seq2seq models [19], have paved the way for methods focused on time series reconstruction and context prediction to learn meaning for representations [20], [21]. Unsupervised learning later became a new paradigm, which not only reduces labeling requirements but also leverages intrinsic temporal patterns to generate labels [22] in certain scenarios.

A recent breakthrough in this field is the application of contrastive learning to time series URL. Learning to distinguish between the positive sample pairs (augmented versions of the same data) and the negative sample pairs (augmented versions of different data) in a way that minimizes the distance between positive pairs and maximizes the distance between negative pairs. [23]. This approach has demonstrated success in various domains, including CV [24]–[27] and time series [6], [9], [28], [29]. Notably, contrastive learning in the context of URL encompasses three levels of learning objectives: instance level [24], [30], [31], cluster (prototype) level [32]–[34], and temporal level [5], [6], [35], each capturing different aspects of similarity and dependency in data.

On time series data, instance-level contrastive learning perturbs original samples, emphasizing the retention of salient features [9]. Prototype-level contrastive learning extends the focus to higher-level semantic information among clusters, offering insights often overlooked by instance level methods [34]. Meanwhile temporal-level contrastive learning captures temporal dependencies surrounding each sample [6].

B. Discriminative Transformations

Researchers have explored transformations to capture different views of time series data. These Techniques helps eliminate noise while preserving key discriminative patterns that might be challenging for a feature extractor directly without additional prior knowledge thus avoid overfitting. Here’s how these techniques achieve this and their impact on avoiding overfitting.

1) *Discrete Fourier Transformation (DFT)*: With the same neural architectures and similar training objectives, URL methods using only DFT transformed time series or only raw data share a small proportion of false prediction during evaluation,

with the rest of them being non-overlapping, revealing relatively independent inductive bias [7].

Fourier transformation decomposes the time series into its frequency components [36], while raw time series data contains information about the temporal trends and fluctuations.

The transformed and raw data offer complementary insights into underlying patterns. False predictions often stem from distinct induction biases introduced by transformations. Merging these views amalgamates their complementary information, bridging the inductive gap caused by their differences.

2) *Continuous Wavelet Transformation (CWT)*: CWT is a tool that provides an overcomplete representation of a signal by letting the translation and scale parameter of wavelets vary continuously [37]. The number primary element used to represent signal (e.g. wavelet with different scale parameters used for transformation) exceeded the minimal necessary number of elements. The abundance and overcompleteness allows analysis with higher accuracy.

Compared to raw time series collapsing spectral features or spectral transformations obscuring temporal stages, Continuous Wavelet Transform (CWT) aligns temporal and spectral patterns in a 2D plane, generating discriminative yet redundant features for URL. However, its high computational time for Multivariate Time Series (MTS) limits its use in time series URL studies.

3) *Encoding Time Series To Image*: [14] proposes a framework to encode time series data as different types of “images” thus allow machines to “visually” recognize and classify time series, which help to extract patterns and structures that more intangible than that can be directly extracted in raw data. For example, using a polar coordinate system, Gramian Angular Field (GAF) images a represented as a Gramian matrix where each element is the trigonometric sum between different time intervals.

Learning methods based on these transformations always leverages a CNN structure to exploit translational invariance within the “images” by extracting features through receptive fields.

4) *Symbolic Transformation*: Symbolic representation techniques like Symbolic Aggregate Approximation (SAX) [38] or Symbolic Fourier Approximation (SFA) [16] transform noisy time series data into abstract symbolic patterns, filtering out noise and reducing classifier overfitting.

SFA, a promising method for time series classification [13], aids in handling high-dimensional, sparse data prone to overfitting. Our approach utilizes these transformations to construct multi-modal views of raw data, guiding the raw MTS encoder to match distributions of crucial patterns extracted by diverse transformation-extractor combinations, addressing challenges related to high-dimensionality, sparsity, and complex pattern interactions in time series data.

C. URL Based on Regularization and Multi-view Learning

Despite successful contrastive learning, the trend leans toward methods integrating multi-modal feature binding and alignment in URL, learning hypotheses from multiple views

of grounded concepts [39], [40]. Regularization-based approaches [41], focus on positive sample pairs to reduce Dirichlet energy, bypassing the curse of dimensionality linked to numerous negative samplings [41]. Theoretical analysis of inductive biases in contrastive and non-contrastive methods involves considering Dirichlet energy on a data augmentation graph [42].

Existing methods leveraging multi-modal features often rely on feature fusion [7], [13]. However, in URL for time series, these approaches, exemplified by [7], focus on domain-specific transformations and fusion strategies without considering semantic relationships across views. Innovations in computer vision (CV), such as [39] and [43], highlight the advantages of aligning and capturing semantic structures across multiple views, a concept yet to be explored in informative time series data.

Unlike existing contrastive learning methods focusing on spectral or temporal domains, our approach aligns multi-modal features from time series samples. By combining learners capturing diverse discriminative patterns, our algorithm learns semantic equivalence more effectively, resulting in stronger theoretical guarantees and outperforming state-of-the-art URL methods.

III. PRELIMINARIES

This section defines the key concepts used in the paper. At first, we define the data type we are interested in, multivariate time series.

A. Unsupervised Representation Learning for Multivariate Time Series

Multivariate time series is a set of variables, containing observations ordered by successive time. We denote a MTS sample with D variables (a.k.a. dimensions or channels) and T timestamps (a.k.a. length) as $x \in \mathbb{R}^{D \times T}$, and a dataset containing N samples as $X = \{x_1, x_2, \dots, x_N\} \in \mathbb{R}^{N \times D \times T}$.

Given a MTS dataset X , the goal of unsupervised representation learning (URL) is to train a neural network model (encoder) $g : \mathbb{R}^{D \times T} \mapsto \mathbb{R}^{D_{repr}}$, the acquired representation $z_i = g(x_i)$ can be informative for downstream tasks, e.g., classification and forecasting. ‘‘Unsupervised’’ means that the labels of downstream tasks are unavailable when training g . To simplify the notation, we denote $Z = g(X) = \{z_1, z_2, \dots, z_N\} \in \mathbb{R}^{N \times D_{repr}}$ in following sections.

B. Neural Encoders And Corresponded Input Features

With respect to raw MTS data and multi-modal features transformed, we denote the features as $x^{(i)} = T^{(i)}(x)$ in this work, i denotes index of the selected transformation operator. The transformed features are highly heterogeneous from the original raw MTS data. Therefore, we designed different neural architectures for the feature encoders w.r.t the multi-modal features, $z^{(i)} = g^{(i)}(x^{(i)})$, they are listed bellow.

1) *Shapelet Learning Neural Network*: Just like CWT, shapelet learning neural network (SLNN) [8] transforms time series signal into energy sequence along with time axis, using a learned wavelet-like small sequence, shapelet, sliding from one side from the signal to another side and outputs distances from the small sequence to the sub sequences of the signal.

Lengths of shapelets vary just like dilating or compressing wavelet to different scales. Allowing SLNN to fit the signal shapes of interest adaptively and automatically search for an optimal temporal-spectral resolution trade of, with the similar idea of CWT. We use SLNN in this work as the raw temporal data feature extractor, $g(\cdot)$.

2) *Convolutional Neural Network*: To extract semantic information from spectral sequences and two-dimensional matrices using local perceptive fields, we utilize one and two-dimensional ResNet CNN architectures as feature extractors. $T^{(img)} : \mathbb{R}^{D \times T} \mapsto \mathbb{R}^{D \times d_w \times d_h}$ represents the transformation operator encoding raw MTS samples into D 2D image-style feature matrices (Sec. II-B3). Similarly, $T^{(dwt)}$ represents the DWT transformation operator generating 2D feature matrices for D channels. Both are accompanied by 2D ResNet encoders, which also include interpolation for ensuring the encoder’s input size $d_w \times d_h$. As for the DFT transformer operator, $T^{(dft)} : \mathbb{R}^{D \times T} \mapsto \mathbb{R}^{D \times T}$, we employ a 1D ResNet as the encoder.

3) *Transformer*: To capture patterns that imply in symbolic features transformed from the raw time series. We take the advantage of the methods that are used in sequence modeling of natural language. Transformers can be used as feature extractors, and they can be pretrained for providing diverse information enhancement. The symbolic transformer operator $T^{(sfa)} : \mathbb{R}^{D \times T} \mapsto \mathbb{R}^{L \times d_e}$ first transforms MTS to token sequences, then the joint the sequences to a long sequence with separators. L denotes the length of the token sequence. Finally, we look up to the word embeddings of the tokens as input of the transformer encoder.

For the sake of simplicity, let us denote $X^{(i)} = T^{(i)}(X) = \{x_1^{(i)}, x_2^{(i)}, \dots, x_N^{(i)}\} \in \mathbb{R}^{N \times \dim T^{(i)}}$ and $Z^{(i)} = g^{(i)}(X^{(i)}) = \{z_1^{(i)}, z_2^{(i)}, \dots, z_N^{(i)}\}$ in subsequent sections. Eventually, we discuss probability density functions (PDF) and eigenfunctions defined on the sample space, which encompasses not only raw data but also transformed features, denoted as $\mathbb{R}^{\text{data}} = \mathbb{R}^{\sum_i \dim T^{(i)}}$.

IV. OVERVIEW

We overview the framework of the proposed multi-modal feature alignment (MMFA) in Section IV. Given the input X , k data transformation, $T^{(i)}(X) = X^{(i)}$, $i \in [k]$, is processed on the raw data, acquiring multi-modal features of the raw data. We denote $X^{(0)} = X$ as alias of the raw MTS data and $T^{(0)}$ as doing no transformations on the raw data. Then we have $F = \{X^{(i)}\}_{i \in [0, k]}$. These transformations help to build up different views about the concepts implied in the raw data and have complemented advantages. Each feature with different modality, such as image, bags of symbols, spectral and temporal features, can capture different aspects

of the same sample. Combining all these modalities can potentially reveals salient patterns appear after transformation thus providing enhanced knowledge about the discriminative patterns.

For the ease of discussion, we divide the encoders to feature extractors and projection matrices, $g^{(i)}(\cdot) = f^{(i)}(\cdot)W$. After getting multi-modal features F , we take the advantage of diverse neural feature extractors, $f^{(0)}, f^{(1)}, \dots, f^{(k)}$, with different architectures and separated parameters w.r.t. raw MTS data and each of the multi-modal features in F that are suitable for the features transformed to different modalities. Then we have $E = [f^{(i)}(X^{(i)})]_{i \in [0, k]} \in \mathbb{R}^{(k+1) \times N \times d_e}$. These feature extractors response differently to noise and discriminative information implied in F . On the one hand, as different extractors is more sensitive to specific noisy patterns, they always shows distinct inductive bias, thus ensembles these extractors showing the potential of filtering out a variety of irrelevant patterns. On the other hand, these transformation preserved discriminative semantic structures in diverse forms and scales, which introduced the need for designing feature extractors with different neural architectures.

For the extracted feature vectors $\mathcal{E} \in \mathbb{R}^{(k+1) \times N \times d_e}$, which is reshaped from $E \in \mathbb{R}^{(k+1) \times N \times d_e}$, we use linear layers, $W \in \mathbb{R}^{d_e \times d_z}$, to transform them to embedding vectors, $\mathcal{Z} = \mathcal{E}W \in \mathbb{R}^{(k+1) \times N \times d_z}$, which recovers local and global spectral embedding methods by leveraging regularization method.

More generally, we treat the transformed features as individual entities in the sample space \mathbb{R}^{data} by splicing the original spaces they lies in directly. This procedure maps the euclidean space \mathbb{R}^{data} to an generic embedding space \mathbb{R}^{d_e} through a non-linear piecewise function $\phi(\cdot) : \mathbb{R}^{\text{data}} \mapsto \mathbb{R}^{d_e}$ which is defined at Eq. 1. $\text{Proj}^{(i)}$ denotes operation that simply splits coordinates of $\mathbb{R}^{\dim T^{(i)}}$ from \mathbb{R}^{data} . Then W maps it linearly to the representation space \mathbb{R}^{d_z} .

$$\phi(X_{\text{data}}^{(i)}) = f^{(i)}(X^{(i)}), X^{(i)} = \text{Proj}^{(i)}(X_{\text{data}}^{(i)}) \quad (1)$$

Just like spectral embedding methods, URL relies on weighted undirected graph $\mathcal{G}(\mathcal{X}, w)$ that indicates semantic equivalence lies in the manifold in the original high dimensional space from where raw data is collected, where $\mathcal{X} \in [(k+1)N]$ denotes the subscript for raw MTS and the transformed features. In this paper, the relation matrix $w \in \mathbb{R}^{(k+1)N \times (k+1)N}$ is constructed by equivalent patterns among features with different modalities and similar patterns lies in each of the feature modalities.

$$w_{ij} =: \begin{cases} \frac{1}{k} p_{T(\mathcal{X}_i), T(\mathcal{X}_j)}(\mathcal{X}_i, \mathcal{X}_j), i \neq j \\ 0, i = j \end{cases} \quad (2)$$

Equation 2 describe semantic equivalence graph \mathcal{G} for approximate reconstruction using low-dimension representations. The probability density function $p_{T(\mathcal{X}_i), T(\mathcal{X}_j)}$ tries to capture the sentimental equivalence between \mathcal{X}_i and \mathcal{X}_j by discovering and matching equivalent patterns leveraging transformation operators $T(\mathcal{X}_i)$ and $T(\mathcal{X}_j)$ jointly, where $T(\mathcal{X}_i)$ denotes the

TABLE I
COMBINATION OF TRANSFORMATION OPERATORS AND NEURAL FEATURE EXTRACTORS.

Transformation Operator	Feature Extractor
Raw Time Series	SLNN
FFT	ResNetId
Image Encoding	ResNet12
CWT	
SFA	LongTransformer
	Pretrained Random

transformation used to acquire the entity \mathcal{X}_i . We further describe two kinds of edges of the graph and corresponded mechanisms about how they contributes to the final utility of the representation in Sec. VI-A. $\frac{1}{k}$ is a normalize factor. An intuitive example for how transformation affects the weights of the graph is shown in Fig. 2.

$$\begin{aligned} & \min_{\theta: W^T \mathcal{E}^T D \mathcal{E} W = I} \text{Tr}(W^T \mathcal{E}^T (D - w) \mathcal{E} W) \\ & = \min_{\theta: \mathcal{Z}^T D \mathcal{Z} = I} \text{Tr}(\mathcal{Z}^T (D - w) \mathcal{Z}) \end{aligned} \quad (3)$$

To generalize the discussion to unseen data, we further discuss how to generalize the LE problem to search representations for infinite new samples sampled according to the distribution, how aligning representations of different transformer-encoder combinations affects connectivity of the nodes in graph \mathcal{G} , and the designation of corresponding training objective in Sec. VI.

Finally, the feature extractor for the raw MTS data is preserved during adaptations for downstream task and inferring process. This raw data feature extractor memorises salient feature extraction methodology knowledge from each of the transformation operators and neural feature extractors during URL training phase. By leveraging shapelet learning neural network, the encoder has low sensitivity with the hyper-parameter configuration for datasets from different domains. The scalability of the method is also promoted by small scale of the neural architecture.

V. TRANSFORMATION OPERATORS AND FEATURE EXTRACTORS SELECTION

In this section, our goal is to leverage previously introduced transformation operators $T^{(i)}, i \in [k]$, to derive multi-modal feature entities capable of revealing salient discriminative patterns. Concurrently, we select neural encoder architectures $g^{(i)}, i \in [k]$, adept at capturing these inherent patterns within the transformed features. This enables the encoders to approximate the eigenfunctions of the semantic equivalence graph, and project input data into a lower-dimensional space which conducive to natural clustering based on pattern occurrence and graph connectivity.

Hence, the process of selecting transformation operators $T^{(i)}$ and their corresponding neural encoders, denoted as

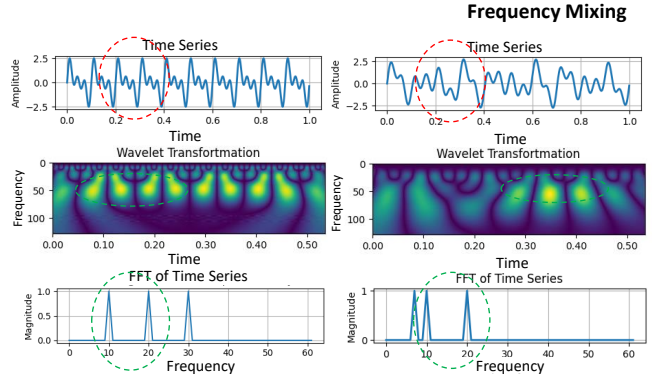
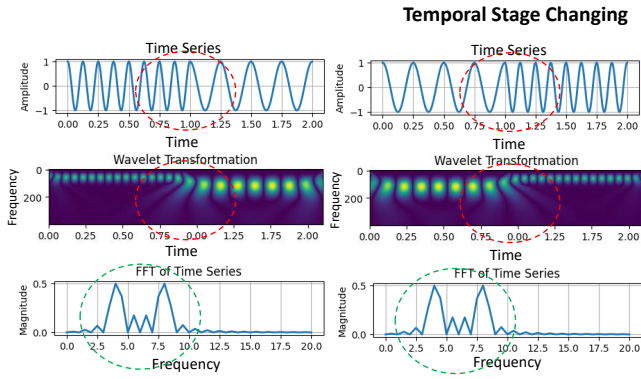


Fig. 2. **Two types of discriminative patterns of interest with three multi-modal feature views.** (raw time series, CWT and FFT of time series) With green dash circle indicating patterns that are similar or hard to distinguish, red dash circle indicating patterns that are easy to distinguish. The feature extractors takes these multi-modal features as input. Difficulties for them to capture certain patterns varies with different transformations, causing different probabilities for them in determining two samples to be semantically identical.

$g^{(i)}(\cdot) = f^{(i)}(\cdot)W$, necessitates assumptions about the discriminative patterns present in the datasets under examination. These assumptions about inductive bias fundamentally address the question of *how an algorithm prioritizes learning one pattern over another*. Consequently, the pivotal principle arises: for datasets exhibiting diverse characteristics and varying sizes, the compatibility of pairings becomes pivotal in providing effective supervisory signals. To streamline, we focus on several potent combinations, detailed in Tab. I.

As discussed in Sec.II, time series data pose complexities in pattern identification and analysis, characterized by heterogeneous feature entities and their diverse patterns. For instance, IMU signals exhibit multiple periodic swings with rapidly varying patterns across different temporal stages [12]. These traits collectively render the signals informative yet challenge pattern extraction. Notably, the DFT directly extracts frequency location patterns in the spectral domain while disregarding temporal stages, emphasizing contributions for certain frequencies across the time axis. Conversely, biological electric signals manifest a blend of frequencies challenging to discern without temporal domain transformations. Specific visual examples illustrating temporal stage changes and frequency mixing are demonstrated in Fig.2.

The selection of feature encoders is generally contingent upon the chosen transformation operator. For instance, we employ CNNs as encoders for FFT and transformations that convert each channel of time series data into a two-dimensional matrix. LongTransformer models are employed to encode symbolic features. Additionally, a neural feature extractor can be trained from scratch or pre-trained with external knowledge injected, as expounded in Sec. VII-B.

Thus, nine combinations of transformation operators and feature extractors, outlined in Tab. I, are designed to hypothesize discriminative features within datasets, introducing varied inductive biases to the primary encoder. In the subsequent subsection, we demonstrate approaches to align representations extracted from each combination and elucidate two mechanisms for MMFA, introducing inductive bias for

Fig. 3. **Edges within and between sub-graphs and how they change the connectivity of the whole graph.** Dashed lines denotes edges with weights of degrees to which the connected vertexes within a sub-graph share similar discriminative patterns. The solid lines indicating edges with weights of probabilities for discover patterns lies in feature of one modality to the other.

enhanced representation learning.

VI. REGULARIZATION BASED MULTI-MODAL FEATURE ALIGNMENT URL TRAINING ALGORITHM

In this section, our aim is to identify semantic measures that can capture all of the inductive biases introduced by all selected transformation operators, feature extractors and semantic equivalence graph \mathcal{G} through unsupervised learning. Initially, we embed the representations into approximated eigenfunctions, each of which partitions the representation space into different clusters. Subsequently, these approximated eigenfunctions contribute to acquiring representations of the input data.

To fulfill these objectives, we devise training objective by treating the supervisory goal as a generalized LE problem. Subsequently, we design an algorithm to minimize the training objective. Consequently, representations encoded from multi-modal features transformed from raw time series are aligned.

A. Design training objective approximating LE problem.

This section aims to formulate the URL problem in a manner akin to a generalized Laplacian Eigenmaps (LE)

approach. Thus, the generalized approach can be applied to the data distribution across the sample space comprising all the transformed features and raw time series. Initially, we establish fundamental concepts closely associated with the LE problem. Subsequently, we align the problem’s objective with the training paradigm introduced in our proposal.

It is assumed that the samples in the dataset and their transformed features are independently and uniformly sampled with a distribution p'_{data} as entities of interest. As discussed in Section V, the selection of the transformation-encoder combinations decides the learners inductive bias respectively, and thus affects the determination of equivalent sample pairs. We construct a distribution for semantic equivalence of pairs of the entities, p_{sim} , whose PDF is defined as a piecewise function, $\frac{1}{k}\pi_{T(x_i), T(x_j)}(x_i, x_j) : \mathbb{R}^{\text{data}} \times \mathbb{R}^{\text{data}} \mapsto \mathbb{R}$, where $T(x_m) = T^{(n)}$ denotes the transformation used to acquire $x_m \in X^{(n)}$. Next, we can generalize \mathcal{G} into a graph describing any of the entities conforms $p'_{\text{data}} : \mathbb{R}^{\text{data}} \mapsto \mathbb{R}$, and weighted edges between them. Since LE problem is strongly related to the concept of Laplacian operator and eigenfunction of it, we next define them in Definition 1 and Definition 2, respectively.

Definition 1. For a function $f : \mathbb{R}^{\text{data}} \mapsto \mathbb{R}$, its Laplacian operator \mathbb{L} is defined as:

$$\begin{aligned} \mathbb{L}(f)(x) &= f(x) + \int_{x'} \frac{\frac{1}{k}\pi_{T(x), T(x')}(x, x')}{p'_{\text{data}}(x)} f(x') dx' \\ &= f(x) + \frac{1}{k} \sum_{i=1}^k \int_{x' \in T^{(i)}(\bar{X})} \frac{\pi_{T(x), T_i}(x, x')}{p'_{\text{data}}(x)} f(x') dx' \end{aligned} \quad (4)$$

Definition 2. If a function f satisfies Eq. 5, the eigenfunction of the Laplacian operator \mathbb{L} with eigenvalue λ :

$$\mathbb{E}_{x \sim p'_{\text{data}}} [(\mathbb{L}(f)(x) - \lambda f(x))^2] = 0 \quad (5)$$

Generally, eigenfunctions with small eigenvalues would correspond to clusters that are almost disconnected from the rest of the graph, which is well-known in the spectral graph theory [44].

Based on this intuition and the Laplacian operator \mathbb{L} definition, FFMA enhances base encoder representations. The chosen transformation-extractor combinations construct sub-graphs from raw MTS, each revealing distinct discriminative patterns. Combining these sub-graphs forms a larger graph, introducing new edges that uncover probabilities of discovering patterns between different combinations. The enhancement occurs through two mechanisms.

Firstly, the transformation-extractor combinations shows the robustness to irrelevant patterns that are introduced by each others. Introducing new edges between sub-graphs can also connect trivial small clusters caused by irrelevant patterns, which increase the cardinality of the irrelevant eigenfunction causing difficulty gaining high performance using representations of a smaller dimension. Secondly, some of the important patterns may be ignored by certain transformation-extractor combination but can be enhanced by another one. The added

edges help to inject this helpful information from one combination to others, providing complementary information gain to the encoder preserved during inference. These added edges are introduced by $\frac{1}{k}\pi_{T(x_i), T(x_j)}(x_i, x_j), i \neq j$. Theorem 1 models more connected components of the graph to eigenvectors by reducing distance between representations of entities at each end of the edges.

Theorem 1. Relationship between Eigenvalues and Distance Reduction in Semantic Similarity.

$\mathbb{E}_{(x, x') \sim p_{\text{sim}}} [(f(x) - f(x'))^2]$ denotes the expected squared difference between representations of semantically similar pairs under a distribution p_{sim} , and f is an eigenfunction of \mathbb{L} . Eq. 6 demonstrates the relationship as follows:

$$\begin{aligned} &\mathbb{E}_{(x, x') \sim p_{\text{sim}}} [(f(x) - f(x'))^2] \\ &= 2\mathbb{E}_{x \sim p'_{\text{data}}} [f(x)^2] - 2\mathbb{E}_{(x, x') \sim p_{\text{sim}}} [f(x)f(x')] \\ &= 2\mathbb{E}_{x \sim p'_{\text{data}}} [f(x)^2] \\ &\quad - 2\mathbb{E}_{(x, x') \sim p'_{\text{data}}} [f(x) \int_{x'} \frac{\frac{1}{k}\pi_{T(x), T(x')}(x, x')}{p'_{\text{data}}(x)} f(x') dx'] \quad (6) \\ &= 2\mathbb{E}_{x \sim p'_{\text{data}}} [f(x)^2] - 2\mathbb{E}_{x \sim p'_{\text{data}}} [(1 - \lambda)f(x)^2] \\ &= 2\lambda\mathbb{E}_{x \sim p'_{\text{data}}} [f(x)^2] \end{aligned}$$

Remark 1. Theorem 1 illustrates that a lower eigenvalue λ correlates with reduced distance between semantically similar pairs. Consequently, minimizing the distance during training aligns the encoder with eigenfunctions of the Laplacian operator possessing small eigenvalues, effectively segregating the graph capturing semantic relations into relatively distinct clusters.

We denote raw MTS samples and its distribution as $x \sim p_{\text{data}}$. X is a group of samples sampled with p_{data} . Then we have $w_{x, T^{(i)}(x)} = 1, x \in X$. To capture the semantic invariance implied in w , the corresponding loss can be estimated and bounded by inequation 7, where $Z \in \mathbb{R}^{(k+1) \times N \times d}$ which is reshaped from \mathcal{Z} and $z_i^{(m)}$ denotes the representation for the i th sample transformed and encoded by $T^{(m)}$ and $g^{(m)}$. To ensure the feasibility of training, we provide an upper-bound of the originally proposed loss function to reduce the training workload, which is demonstrated at Theorem 2.

Theorem 2. Semantic Invariance Estimation Theorem.

$x \sim p_{\text{data}}$ denotes raw Multivariate Time Series (MTS) samples, where X represents a group of samples sampled with p_{data} . Assuming $\pi_{T^{(i)}, T^{(j)}}(T^{(i)}(x), T^{(j)}(x)) = 1, x \in X$ to capture the semantic invariance implied in w , the corresponding loss, denoted by $\mathcal{L}'_{\text{inv}}(Z)$, can be estimated and bounded as shown in Inequality 7.

$$\begin{aligned} \mathcal{L}'_{\text{inv}}(Z) &= \frac{1}{Nk(k+1)} \sum_{\substack{m=0 \\ m \neq n}}^k \sum_{i=1}^N \|z_i^{(m)} - z_i^{(n)}\|_2^2 \\ &\leq \frac{2}{N(k+1)} \sum_{i=1}^N \sum_{m=1}^k \|z_i^{(0)} - z_i^{(m)}\|_2^2 \end{aligned} \quad (7)$$

The expression $\mathcal{L}'_{inv}(Z)$ signifies the optimization objective aimed at capturing semantic invariance among the multi-modal features.

Proof. The proof of this theorem follows from the established inequalities detailed in Inequation 8.

$$\begin{aligned}
\mathcal{L}'_{inv}(Z) &= \frac{1}{Nk(k+1)} \sum_{i=1}^N \left(2 \sum_{m=1}^k \|z_i^{(0)} - z_i^{(m)}\|_2^2 \right. \\
&\quad \left. + \sum_{\substack{m=1, n=1 \\ m \neq n}}^k \|z_i^{(m)} - z_i^{(n)}\|_2^2 \right) \\
&\leq \frac{1}{Nk(k+1)} \sum_{i=1}^N \left[2 \sum_{m=1}^k \|z_i^{(0)} - z_i^{(m)}\|_2^2 \right. \\
&\quad \left. + \sum_{\substack{m=1, n=1 \\ m \neq n}}^k (\|z_i^{(0)} - z_i^{(m)}\|_2^2 + \|z_i^{(0)} - z_i^{(n)}\|_2^2) \right] \\
&= \frac{2}{N(k+1)} \sum_{i=1}^N \sum_{m=1}^k \|z_i^{(0)} - z_i^{(m)}\|_2^2
\end{aligned} \tag{8}$$

□

Proposal 1. According to the Theorem 2, we define $\mathcal{L}_{inv}(Z)$ as the optimization objective capturing semantic invariance among the multi-modal features.

$$\mathcal{L}_{inv}(Z) = \frac{1}{N(k+1)} \sum_{i=1}^N \sum_{m=1}^k \|z_i^{(0)} - z_i^{(m)}\|_2^2 \tag{9}$$

Lemma 1. Orthogonality and Maximization of Information in Eigenfunction-Based Representations.

For $\forall g, h : \mathbb{R}^{data} \mapsto \mathbb{R}$, $\mathbb{E}x \sim p'_{data}[\mathbb{L}(g)(x) \cdot h(x)] = \mathbb{E}x \sim p'_{data}[g(x) \cdot \mathbb{L}(h)(x)]$. Therefore, \mathbb{L} is a symmetric linear operator. The representations are outputs derived from approximated eigenfunctions of \mathbb{L} possessing low eigenvalues, $f_{rep}(\cdot) = [f_1(\cdot), f_2(\cdot), \dots, f_k(\cdot)]^T$, and \mathbb{L} is a symmetric real value linear operator. According to spectral theorem [44], it is imperative to ensure orthogonality while maximizing the overall information:

$$\mathbb{E}x \sim p'_{data}[f_{rep}(x)f_{rep}(x)^T] = \mathbb{I} \tag{10}$$

Proposal 2. According to Lemma 1, we design two relevant losses, \mathcal{L}_{var} and \mathcal{L}_{cov} , in Eq. 11 Eq. 12.

$$\begin{aligned}
\mathcal{L}_{var}(Z) &= \frac{1}{(N-1)kd} \sum_{l=1}^k \sum_{m \neq n}^N \left[\sum_{i=1}^n (z_i^{(l)} - \bar{z}^{(l)})(z_i^{(l)} - \bar{z}^{(l)})^T \right]_{m,n} \\
\text{where } \bar{z}^{(l)} &= \frac{1}{n} \sum_{i=1}^n z_i^{(l)}
\end{aligned} \tag{11}$$

$$\mathcal{L}_{cov}(Z) = \frac{1}{dN} \sum_{l=0}^k \sum_{i=1}^N \sum_{j=1}^d \max(0, 1 - \sqrt{\text{Var}(z_{i,j}^{(0)}) + \epsilon}) \tag{12}$$

Proposal 3. According to Proposal 1 and Proposal 2, the end-to-end training object is obtained in equation 13. α , β and γ are empirical parameters.

$$\mathcal{L} = \alpha \mathcal{L}_{cov} + \beta \mathcal{L}_{var} + \gamma \mathcal{L}_{inv} \tag{13}$$

B. Asymmetric Encoders Alignment Optimizing algorithm

We finally design Algorithm 1 minimizing the training objective by mini-batch gradient descent. After the transformation-extractor combination is initialized, for each iteration, the gradients for each of the terms of the training objective is accumulated w.r.t each of the encoder. We note that the transformation can be performed in a off-line manner, thus making it convenient for taking advantage of time consuming transformations.

Algorithm 1: Asymmetric neural encoders alignment

Data: D : MTS dataset; $T^{(i)}, i \in [k]$: transformation operators; $g^{(i)}, i \in [k]$: neural encoder architecture.
Result: g : Trained SLNN encoder for MTS representation.

- 1 $\theta_g \leftarrow$ initialized parameters of the raw MTS encoder.
- 2 **for** i in $[k]$ **do**
- 3 $\theta_{g^{(i)}} \leftarrow$ initialized parameters of the encoders w.r.t $T^{(i)}$.
- 4 **for** iteration = 1, 2... **do**
- 5 $X \leftarrow$ sample a mini-batch of samples from D .
- 6 **for** i in $[k]$ **do**
- 7 $X^{(i)} \leftarrow T^{(i)}(X)$ # transform raw MTS
- 8 $\theta_{\bar{g}}, \theta_{\bar{g}^{(i)}} \leftarrow U(g, g^{(i)}, X, X^{(i)})$ # accumulate gradients
- 9 $\theta_{g^{(i)}} \leftarrow \theta_{g^{(i)}} + \epsilon \frac{1}{k} (\theta_{\bar{g}^{(i)}} - \theta_{g^{(i)}})$ # update encoder
- 10 $\theta_g \leftarrow \theta_g + \epsilon (\theta_{\bar{g}} - \theta_g)$ # update encoder
- 11 **return** g

Algorithm 1 takes the MTS dataset D , a set of transformation operators $T^{(i)}$ and corresponded neural architecture for the encoders as input. Then the parameters of the encoders g and $g^{(i)}$ are initialized in line 1-3. In line 7-9, update step U is defined as $U(g, g^{(i)}, X, X^{(i)}) = \theta - \nabla_{\theta} \mathcal{L}([g^{(i)}(X^{(i)}), g(X)])$, where θ denotes the parameters of the two encoders. We divides the designed training objective into k parts, iteratively computes and accumulates gradient for both g and $g^{(i)}$. After accumulates all the gradients of the batch, the encoder g is updated.

We employs a multi-stage learning approach to align the representations learned by individual encoders with the main time series encoder, thereby facilitating the creation of a cohesive and informative representation of MTS data suitable for downstream tasks.

After the training phase, we only need to preserve the encoder, g , for raw MTS and adapt it to diverse downstream tasks.

VII. EXPERIMENTS

In this section, we conduct extensive experiments to demonstrate the performance of the proposed approach.

A. Experimental Settings

We perform extensive experiments on a total of 34 real-world datasets to comprehensively analyze the quality of MMFA representations across diverse patterns. Our investigation encompasses three primary tasks, supervised classification, unsupervised clustering, and anomaly detection. It is noteworthy that in the case of anomaly detection, the MTS representation is considered at the segment level (as opposed to observation-level [45], [46]).

Specifically, we consider a series within each sliding window $x_i[t, t + w], t \in [N - w + 1]$ as anomalous if it contains at least one abnormal observation. To address these tasks, we train popular models such as SVM, K-means, and Isolation Forest on the acquired representations. The datasets, baseline methods, implementations, and evaluation metrics are presented for clarity.

1) *Datasets*: To assess the representation quality across three downstream tasks, we employ 30 diverse MTS datasets. These datasets exhibit variations in sample size, dimensionality, length, number of classes, and application scenarios. The default train/test split is applied uniformly across all datasets, with the encoder and task-specific models exclusively trained on the training samples. The specific datasets utilized for each task are outlined below. The original datasets’ dimensionalities (channel numbers) can overwhelm 2D transformations (e.g., rp, dwt) and ResNet encoders due to limited computation resources. Therefore, we perform average pooling on transformed multi-channel 2D features, capping dataset channels at 64. Raw time series channels remain unchanged for input into the time series encoder.

Classification. We assess the performance of MTS categorization across all 30 datasets from the widely used UEA archive [12]. These datasets encompass diverse domains such as human action recognition, Electrocardiography monitoring, and audio classification [12]. The statistical details of the datasets can be found in Tab. II.

Clustering. In line with a recent study on clustering multivariate time series, we assess the performance of clustering using 12 diverse UEA subsets. These subsets exhibit significant heterogeneity in terms of training/test set sizes, length, as well as the number of dimensions and classes. The statistics for these 12 datasets are shown in Tab. II (denoted by *).

Anomaly Detection. In this study, we leverage four recently released datasets sourced from diverse real-world applications to perform anomaly detection. The datasets include anomaly data from the Soil Moisture Active Passive satellite (SMAP) and the Mares Science Laboratory rover (MSL), both obtained through NASA [48]. Additionally, we utilize the Server Machine Data (SMD), a dataset spanning five weeks, collected by [46] from a major Internet company. The Application Server Dataset (ASD) covers a period of 45 days and characterizes the server’s status, recently compiled

TABLE II
STATISTICS ON THE 30 UEA DATASETS ARE EMPLOYED FOR CLASSIFICATION ASSESSMENT, WHILE 12 SPECIFIC SUBSETS (DENOTED BY *) UNDERGO CLUSTERING EVALUATION AS PER THE METHODOLOGY OUTLINED IN [47].

Dataset	# Train	# Test	# Dim	Length	# Class
ArticularyWordRecognition*	275	300	9	144	25
AtrialFibrillation*	15	15	2	640	3
BasicMotions*	40	40	6	100	4
CharacterTrajectories	1422	1436	3	182	20
Cricket	108	72	6	1197	12
DuckDuckGeese	50	50	1345	270	5
EigenWorms	128	131	6	17984	5
Epilepsy*	137	138	3	206	4
EthanolConcentration	261	263	3	1751	4
ERing*	30	270	4	65	6
FaceDetection	5890	3524	144	62	2
FingerMovements	316	100	28	50	2
HandMovementDirection*	160	74	10	400	4
Handwriting	150	850	3	152	26
Heartbeat	204	205	61	405	2
InsectWingbeat	30000	20000	200	30	10
JapaneseVowels	270	370	12	29	9
Libras*	180	180	2	45	15
LSST	2459	2466	6	36	14
MotorImagery	278	100	64	3000	2
NATOPS*	180	180	24	51	6
PenDigits*	7494	3498	2	8	10
PEMS-SF*	267	173	963	144	7
Phoneme	3315	3353	11	217	39
RacketSports	151	152	6	30	4
SelfRegulationSCP1	268	293	6	896	2
SelfRegulationSCP2	200	180	7	1152	2
SpokenArabicDigits	6599	2199	13	93	10
StandWalkJump*	12	15	4	2500	3
UWaveGestureLibrary*	120	320	3	315	8

by [45]. Following the methodology outlined in [45], we evaluate SMD using 12 entities unaffected by concept drift. The dataset statistics are shown in Tab. IV.

2) *Baselines*: We use 21 baselines for comparison, which are divided into two groups:

URL methods. We compare our MMFA framework with 6 time series URL baselines, including TS2Vec [9], T-Loss [28], TNC [5], TS-TCC [6], TST [10] and CSL [8]. All URL competitors are evaluated in the same way as MMFA for a fair comparison.

Methods tailored to specific tasks. We also incorporate benchmarks customized for downstream tasks. We opt for distinguished strategies in classification, including the widely-used baseline DTWD [12]. DTWD employs a one-nearest-neighbor classifier with dynamic time warping as the distance metric. Additionally, we consider five supervised techniques: MLSTM-FCNs [49] utilizing recurrent neural networks, TapNet [50] employing attentional prototypes, ShapeNet [51] based on shapelets, and CNN-based models OSCNN [52] and DSN [53]. To ensure a fair comparison, we exclude ensemble methods such as those outlined in [54]. It is worth noting that the supervised classification methods leverage true labels for feature learning, akin to data augmentation or sampling in URL. Hence, the fairness of the comparison between MMFA and the baselines is maintained.

We assess six sophisticated clustering benchmarks, including dimension-reduction-based MC2PCA [55] and TCK [56], distance-based m-kAVG+ED and m-kDBA [57],

deep learning-based DeTSEC [58], and shapelet-based MUSLA [47].

Since no documented anomaly detection evaluations in segment-level settings exist, we create two raw MTS baselines using Isolation Forest for fair comparisons, models operating at each timestamp (IF-s).

3) *Evaluation Metrics.*: Standard metrics are used to assess downstream task performance. Accuracy (Acc) [12] is applied for classification tasks. Clustering outcomes are measured using Rand Index (RI) and Normalized Mutual Information (NMI) [47], [59]. Anomaly detection employs F1-score [45].

4) *Implementation Details.*: The MMFA framework is implemented using PyTorch 1.10.2, and all experiments run on a Ubuntu machine equipped with Tesla A100 GPUs. Data augmentation methods are implemented using tsaug [60] with default parameters.

The majority of MMFA’s hyperparameters are consistently assigned fixed values across all experiments, devoid of any hyperparameter optimization. The coefficients α and β in Eq. 13 are both assigned a value of 25, while γ is set to 1. Additionally, ϵ takes on the value of 10^{-7} in Eq. 12. The SGD optimizer is employed to train all feature encoders with a learning rate fixed at 10^{-4} .

For simplicity, to discover high-performance transformation-encoder combinations for each of the datasets, we treat the raw time series encoder as the **main encoder**, and evaluate the rest of each of the combinations in Tab. I, respectively. Then, the main encoder and the rest top-3 encoders are trained together according to Alg. 1.

Finally, we report the highest performance. For all datasets, the batch size is uniformly set to 8. In the context of anomaly detection tasks, the parameter d assumes values of 240, 320, 32, and 32 for SMAP, MSL, SMD, and ASL, respectively.

We reproduce the time series URL baseline by employing the publicly available code provided by the original authors, configured as recommended. The classification baselines and task-specific clustering baselines’ outcomes are extracted from the cited publications [9], [12], [47], [51]–[53]. Our reproduced results cover other aspects.

B. Empirical Analysis

In this study, we focus on time series URL, aiming to extract structured features from unlabeled data. Our goal is to evaluate unsupervised representation learning methods’ efficacy, robustness, and adaptability across diverse datasets and domains. Through experiments, we aim to scrutinize algorithms, assess scalability, and compare them to the proposed MMFA framework, outlined by our research questions (RQs).

RQ 1. *How does FFMA framework perform compared to other unsupervised methods?*

Tab. III, Tab. V, and VI show the comparison results for classification, clustering, and anomaly detection tasks. The proposed FFMA framework consistently outperforms unsupervised competitors across most tasks and datasets, demonstrating superior overall performance. Specifically, MMFA

achieves the highest accuracy in 18 out of 30 datasets, ranking the best among all baselines. Moreover, MMFA surpasses all unsupervised methods in total dataset wins, aligning with expectations due to its capability to inject cross-modal knowledge into the time series encoder, leveraging diverse feature engineering techniques.

For a fair comparison, we crafted a variant of MMFA, denoted as FFMA-aug, solely employing data augmentations: jittering, cropping, warping, and quantizing pooling, with the same time series encoder. FFMA’s performance significantly surpassed FFMA-aug, thanks to denoising effects and the extraction of salient patterns by various transformations and neural encoders, as detailed in Sec. VI. This integration empowered FFMA to induce more extensive discriminative patterns.

The clustering results are displayed in Tab. V. MMFA surpasses all competitors except for PenDigits and AtrialFibrillation datasets. For PenDigits (length 8), MMFA demonstrates limitations in learning from short time series, as transformations struggle to capture significant patterns.

Feature engineering techniques extract patterns enhancing discrimination or comprehension of data, surpassing simple data augmentation. Effective methods in MMFA emphasize pertinent information while reducing noise, yielding robust representations resilient to irrelevant data variations.

RQ 2. *How does FFMA framework perform compared to the supervised approaches?*

It is surprising that MMFA achieves better accuracy than tailored fully supervised competitors for time series classification, indicating its extraction of richer information directly from raw time series during inference.

Unsupervised methods efficiently leverage intrinsic structure of data without task-specific tuning, enhancing feature extraction capabilities that go beyond specific tasks, fostering holistic data understanding and potential transferability. These methods are label-free, automating the discovery of latent structures and relationships within data, revealing insights not apparent in supervised techniques reliant on predefined labels.

In Sec. VI, we showcase MMFA’s capacity to discern patterns, significantly contributing to uncovering hidden structures and providing novel data perspectives.

RQ 3. *How does the impact of data characteristics?*

In our analysis, the evaluated datasets exhibit significant variations in training dataset sizes, numbers of channels, time series length, and salient patterns. Tab. II illustrates the diversity: training set sizes range from 12 (StandWalkJump, comprising 3 classes with only 4 samples per class, constituting a 3-way, 4-shot learning task) to 30,000 (InsectWingbeat, characterized by abundant training samples). Consequently, we conduct correlation analysis on the UEA datasets focusing on these three data characteristics and show the findings in Fig. 4.

As depicted in (a) of Fig. 4, MMFA exhibits a lower rank with smaller training sets. Upon closer examination of larger datasets, such as UWaveGestureLibrary and InsectWingbeat,

TABLE III
COMPARISONS OF PERFORMANCE IN MTS CLASSIFICATION. THE TOP-PERFORMING RESULTS OF URL METHODS ARE SHOWN IN BOLD, WITH † DENOTING THE OVERALL BEST PERFORMANCE.

Dataset	Tailored Classification Approaches						Unsupervised Representation Learning + Classifier							
	DTWD	MLSTM-FCNs	TapNet	ShapeNet	OSCNN	DSN	TS2Vec	T-Loss	TNC	TS-TCC	TST	CSL	MMFA-aug	MMFA
ArticularyWordRecognition	0.987	0.973	0.987	0.987	0.988	0.984	0.987	0.943	0.973	0.953	0.977	0.990	0.973	0.993 †
AtrialFibrillation	0.200	0.267	0.333	0.400	0.233	0.067	0.200	0.133	0.133	0.267	0.067	0.533 †	0.533 †	0.533 †
BasicMotions	0.975	0.950	1.000†	1.000†	1.000†	1.000†	0.975	1.000 †	0.975	1.000 †	0.975	1.000 †	1.000 †	1.000 †
CharacterTrajectories	0.989	0.985	0.997	0.980	0.998†	0.994	0.995	0.993	0.967	0.985	0.975	0.991	0.987	0.991
Cricket	1.000†	0.917	0.958	0.986	0.993	0.989	0.972	0.972	0.958	0.917	1.000 †	0.994	0.986	1.000 †
DuckDuckGeese	0.600	0.675	0.575	0.725†	0.540	0.568	0.680	0.650	0.460	0.380	0.620	0.380	0.620	0.680
EigenWorms	0.618	0.504	0.489	0.878†	0.414	0.391	0.847	0.840	0.840	0.779	0.748	0.779	0.768	0.779
Epilepsy	0.964	0.761	0.971	0.987	0.980	0.999†	0.964	0.971	0.957	0.957	0.949	0.986	0.899	0.987 †
ERing	0.133	0.133	0.133	0.133	0.882	0.922	0.874	0.133	0.852	0.904	0.874	0.967 †	0.922	0.930
EthanolConcentration	0.323	0.373	0.323	0.312	0.241	0.245	0.308	0.205	0.297	0.285	0.262	0.498 †	0.331	0.361
FaceDetection	0.529	0.545	0.556	0.602	0.575	0.635†	0.501	0.513	0.536	0.544	0.534	0.593	0.526	0.555
FingerMovements	0.530	0.580	0.530	0.580	0.568	0.492	0.480	0.580	0.470	0.460	0.560	0.590	0.490	0.610 †
HandMovementDirection	0.231	0.365	0.378	0.338	0.443	0.373	0.338	0.351	0.324	0.243	0.243	0.432	0.351	0.487 †
Handwriting	0.286	0.286	0.357	0.451	0.668†	0.337	0.515	0.451	0.249	0.498	0.225	0.533	0.370	0.472
Heartbeat	0.717	0.663	0.751	0.756	0.489	0.783†	0.683	0.741	0.746	0.751	0.746	0.722	0.720	0.761
InsectWingbeat	N/A	0.167	0.208	0.250	0.667†	0.386	0.466	0.156	0.469	0.264	0.105	0.256	0.425	0.469
JapaneseVowels	0.949	0.976	0.965	0.984	0.991†	0.987	0.984	0.989	0.978	0.930	0.978	0.919	0.960	0.978
Libras	0.870	0.856	0.850	0.856	0.950	0.964†	0.867	0.883	0.817	0.822	0.656	0.906	0.833	0.894
LSST	0.551	0.373	0.568	0.590	0.413	0.603	0.537	0.509	0.595	0.474	0.408	0.617 †	0.372	0.451
MotorImagery	0.500	0.510	0.590	0.610†	0.535	0.574	0.510	0.580	0.500	0.610	0.500	0.610	0.510	0.630 †
NATOPS	0.883	0.889	0.939	0.883	0.968	0.978†	0.928	0.917	0.911	0.822	0.850	0.878	0.900	0.933
PEMS-SF	0.711	0.699	0.751	0.751	0.760	0.801	0.682	0.676	0.699	0.734	0.740	0.827	0.827	0.838 †
PenDigits	0.977	0.978	0.980	0.977	0.986	0.987	0.989 †	0.981	0.979	0.974	0.560	0.990 †	0.979	0.980
PhonemeSpectra	0.151	0.110	0.175	0.298	0.299†	0.320	0.233	0.222	0.207	0.252	0.085	0.255 †	0.183	0.216
RacketSports	0.803	0.803	0.868	0.882†	0.877	0.862	0.855	0.855	0.776	0.816	0.809	0.882 †	0.815	0.862
SelfRegulationSCP1	0.775	0.874	0.652	0.782	0.835	0.717	0.812	0.843	0.799	0.823	0.754	0.846	0.887	0.901 †
SelfRegulationSCP2	0.539	0.472	0.550	0.578	0.532	0.464	0.578	0.539	0.550	0.533	0.550	0.496	0.617	0.628 †
SpokenArabicDigits	0.963	0.990	0.983	0.975	0.997†	0.991	0.988	0.905	0.934	0.970	0.923	0.990	0.980	0.990
StandWalkJump	0.200	0.067	0.400	0.533	0.383	0.387	0.467	0.333	0.400	0.333	0.267	0.667 †	0.667 †	0.667 †
UWaveGestureLibrary	0.903	0.891	0.894	0.906	0.927	0.916	0.906	0.875	0.759	0.753	0.575	0.922	0.922	0.931 †
Avg Acc														
incl. InsectWingbeat	/	0.621	0.657	0.699	0.704	0.691	0.704	0.657	0.670	0.668	0.617	0.735	0.712	0.750 †
excl. InsectWingbeat	0.650	0.637	0.673	0.714	0.706	0.701	0.712	0.675	0.678	0.681	0.635	0.751	0.722	0.760 †
Avg Ranking (URL only)	/	/	/	/	/	/	3.93	4.60	5.37	5.23	6.20	2.70	4.40	1.90
Avg Ranking (All)	9.47	9.40	6.87	5.40	5.37	5.80	6.80	7.83	9.33	9.03	10.43	4.26	7.13	3.10 †

TABLE IV
STATISTICS OF EVALUATED ANOMALY DETECTION DATASETS.

Dataset	# Entity	# Dim	Train length	Test length	Anomaly ratio (%)
SMAP	55	25	135183	427617	13.13
MSL	27	55	58317	73729	10.72
SMD	12	38	304168	304174	5.84
ASL	12	19	102331	51840	4.61

where MMFA achieves a higher rank, it aligns closely with the methods exhibiting superior performance. These observations suggest that MMFA excels in achieving higher few-shot performance.

Limited correlation exists between classification performance rank and dataset dimensionality, showcasing MMFA’s stability across varying channel counts in time series. Conversely, negative correlations between rank and time series length indicate MMFA’s stronger adaptability to longer time series compared to baselines. However, a limitation can be observed that MMFA struggles with shorter time series (e.g., PenDigits datasets with length = 8), evident in lower performance across classification and clustering tasks. This limitation may stem from transformation nature, requiring optimal performance from time series of specific lengths.

RQ 4. How does the utilization of pretraining impact unsupervised time series representation learning compared to non-pretrained models?

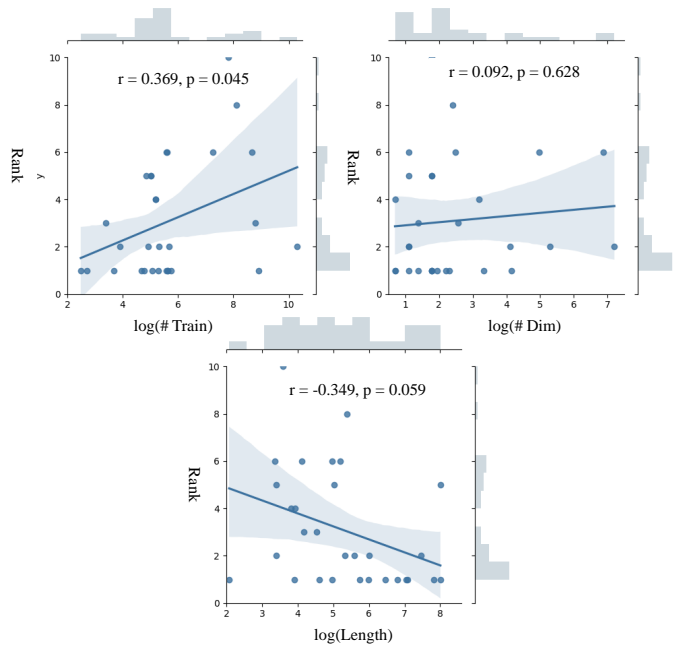


Fig. 4. Correlation plot for classification performance rank of FFMA on 30 UEA datasets, train size, time series dimensionality and time length. Logarithms are used to improve linearity.

TABLE V
THE MTS CLUSTERING COMPARISON IDENTIFIES THE MOST EFFECTIVE RESULTS FROM URL METHODS IN BOLD, WITH † INDICATING SUPERIORITY OVER OTHERS.

Dataset	Metric	Tailored Clustering Approaches						Unsupervised Representation Learning + Clustering							
		MC2PCA	TCK	m-kAVG+ED	m-kDBA	DeTSEC	MUSLA	TS2Vec	T-Loss	TNC	TS-TCC	TST	CSL	MMFA-aug	MMFA
ArticularyWordRecognition	RI	0.989	0.973	0.952	0.934	0.972	0.977	0.980	0.975	0.938	0.946	0.978	0.990	0.990	0.998 †
	NMI	0.934	0.873	0.834	0.741	0.792	0.838	0.880	0.842	0.565	0.621	0.866	0.942	0.942	0.983 †
AtrialFibrillation	RI	0.514	0.552	0.705	0.686	0.629	0.724	0.465	0.469	0.518	0.469	0.444	0.743 †	0.524	0.524
	NMI	0.514	0.191	0.516	0.317	0.293	0.538	0.080	0.149	0.147	0.164	0.171	0.587 †	0.251	0.251
BasicMotions	RI	0.791	0.868	0.772	0.749	0.717	1.000 †	0.854	0.936	0.719	0.856	0.844	1.000	0.845	1.000
	NMI	0.674	0.776	0.543	0.639	0.800	1.000 †	0.820	0.871	0.394	0.823	0.810	1.000	0.806	1.000
Epilepsy	RI	0.613	0.786	0.768	0.777	0.840	0.816	0.706	0.705	0.650	0.736	0.718	0.873	0.679	0.876 †
	NMI	0.173	0.534	0.409	0.471	0.346	0.601	0.312	0.306	0.156	0.451	0.357	0.705	0.530	0.721 †
ERing	RI	0.756	0.772	0.805	0.775	0.770	0.841	0.925	0.885	0.764	0.821	0.867	0.968	0.968	0.972 †
	NMI	0.336	0.399	0.400	0.406	0.392	0.722	0.775	0.672	0.346	0.478	0.594	0.906	0.906	0.918 †
HandMovementDirection	RI	0.627	0.635	0.697	0.685	0.628	0.719†	0.609	0.599	0.613	0.608	0.607	0.651	0.630	0.657
	NMI	0.067	0.103	0.168	0.265	0.112	0.398†	0.044	0.034	0.051	0.053	0.039	0.175	0.118	0.185
Libras	RI	0.892	0.917	0.911	0.913	0.907	0.941	0.904	0.922	0.896	0.881	0.886	0.941	0.938	0.944 †
	NMI	0.577	0.620	0.622	0.622	0.602	0.724	0.542	0.654	0.464	0.373	0.400	0.761	0.730	0.785 †
NATOPS	RI	0.882	0.833	0.853	0.876	0.714	0.976†	0.817	0.836	0.700	0.792	0.809	0.876	0.850	0.919
	NMI	0.698	0.679	0.643	0.643	0.043	0.855†	0.523	0.558	0.222	0.513	0.565	0.657	0.628	0.864
PEMS-SF	RI	0.424	0.191	0.817	0.755	0.806	0.892†	0.765	0.746	0.763	0.789	0.726	0.858	0.842	0.569 †
	NMI	0.011	0.066	0.491	0.402	0.425	0.614†	0.290	0.102	0.278	0.331	0.026	0.537	0.528	0.619 †
PenDigits	RI	0.929	0.922	0.935	0.881	0.885	0.946	0.941	0.936	0.873	0.857	0.818	0.950	0.921	0.932
	NMI	0.713	0.693	0.738	0.605	0.563	0.826†	0.776	0.749	0.537	0.339	0.090	0.822	0.703	0.730
StandWalkJump	RI	0.591	0.762	0.733	0.695	0.733	0.771†	0.410	0.410	0.457	0.589	0.467	0.724	0.591	0.761
	NMI	0.350	0.536	0.559	0.466	0.556	0.609†	0.213	0.213	0.193	0.187	0.248	0.554	0.336	0.611
UWaveGestureLibrary	RI	0.883	0.913	0.920	0.893	0.879	0.913	0.865	0.893	0.817	0.796	0.779	0.927	0.927	0.929 †
	NMI	0.570	0.710	0.713	0.582	0.558	0.728	0.511	0.614	0.322	0.215	0.244	0.731	0.731	0.749 †
Avg.	RI	0.741	0.760	0.822	0.801	0.790	0.876†	0.770	0.776	0.726	0.762	0.745	0.875	0.809	0.875
	NMI	0.468	0.515	0.553	0.513	0.457	0.704†	0.480	0.480	0.306	0.379	0.366	0.698	0.601	0.710
Avg Ranking (URL only)		/	/	/	/	/	/	5.08	5.25	6.92	6.08	5.92	1.75	3.25	1.33 †
Avg Ranking (All)		8.83	7.75	6.58	7.58	9.17	2.92	9.00	8.67	12.58	10.75	10.42	2.58	5.41	2.00 †

TABLE VI
COMPARISON OF PERFORMANCE IN ANOMALY DETECTION OF MTS. SLIDING WINDOW’S LENGTH IS SET TO 100, WITH THE MOST OPTIMAL OUTCOMES HIGHLIGHTED IN BOLD.

Dataset	IF-s	IF-p	TS2Vec	T-Loss	TNC	TS-TCC	TST	csl	MMFA-aug	MMFA
SMAP	0.0890	0.2166	0.2834	0.3862	0.3218	0.3501	0.2511	0.4049	0.2654	0.4142
MSL	0.0077	0.2653	0.1753	0.2771	0.2629	0.3074	0.2645	0.4033	0.3325	0.3923
SMD	0.2912	0.2152	0.2846	0.2472	0.2291	0.2454	0.1859	0.2784	0.3525	0.4027
ASD	0.2585	0.3193	0.3735	0.3449	0.2945	0.2679	0.2926	0.4349	0.3722	0.4626
Avg F1-score	0.1616	0.2541	0.2792	0.3139	0.2771	0.2927	0.2485	0.3804	0.3307	0.4180
Avg Ranking	8.25	7.50	5.50	4.75	7.00	6.00	8.25	2.50	4.00	1.25

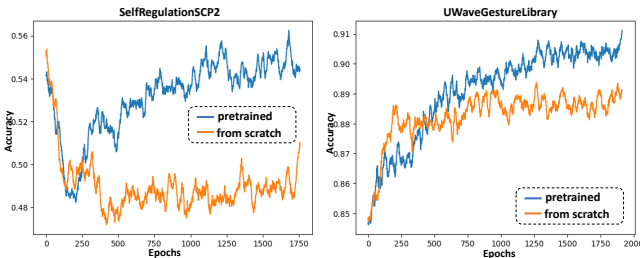


Fig. 5. **Pretrained LongTransformer v.s LongTransformer trained from scratch.** In addition to raw time series and its encoder, we only choose SFA and pretrained or non-pretrained LongTransformer as the combination for transformation and neural encoder, which are demonstrated in I on SelfRegulationSCP2 and UWaveGestureLibrary dataset. It is shown in the figure that pretrained LongTransformer finally gain much higher performance.

We conducted experiments comparing the performance of a pretrained LonTransformer model against a non-pretrained LonTransformer model for time series representation learning. Initially, the time series data was transformed into symbolic word bags. Our approach aimed to assess how pretraining, specifically via the Word-Word Masking (WWM) task, influenced unsupervised time series representation learning.

The findings show that pretraining significantly boosts unsupervised time series representation learning compared

to non-pretrained models. Despite the slower convergence of the pretrained LonTransformer model shown in Fig. 5, it ultimately outperformed the non-pretrained version by a wide margin, demonstrating the effectiveness of leveraging knowledge from the WWM task. This performance boost probably due to the BERT encoder’s capacity to identify patterns between the WWM-pretrained corpus and symbolic features from time series data. Overall, these results highlight the value of pretraining in enhancing the extraction of meaningful representations from time series data.

VIII. CONCLUSION AND FUTURE DIRECTIONS

In this study, we propose a framework aimed at mitigating the limitations arising from intrinsic feature engineering in Universal Representation Learning (URL) for Multivariate Time Series (MTS). Our model-agnostic approach offers a high utility and scalable representation encoder learning paradigm. The incorporation of feature alignment and regularization methods forms a novel URL framework, surpassing existing state-of-the-art approaches.

Looking ahead, this study unveils several promising avenues. For instance, delving deeper into refining graph alignment and connectivity could yield even more precise and comprehensive representations. The integration of broader external knowledge or domain-specific information holds the potential to further enrich these representations. Additionally, exploring the transferability of these methods could unveil broader applications and enhance their generalizability.

REFERENCES

- [1] S. Bennett, M. Cucuringu, and G. Reinert, "Detection and clustering of lead-lag networks for multivariate time series with an application to financial markets," 2022.
- [2] E. Kim, S. Cho, B. Lee, and M. Cho, "Fault detection and diagnosis using self-attentive convolutional neural networks for variable-length sensor data in semiconductor manufacturing," *IEEE Transactions on Semiconductor Manufacturing*, vol. 32, no. 3, pp. 302–309, 2019.
- [3] A. Riley and E. Nica, "Internet of things-based smart healthcare systems and wireless biomedical sensing devices in monitoring, detection, and prevention of covid-19," *American Journal of Medical Research*, vol. 8, no. 2, 2021.
- [4] K. Bi, L. Xie, H. Zhang, X. Chen, X. Gu, and Q. Tian, "Accurate medium-range global weather forecasting with 3d neural networks," *Nature*, pp. 1–6, 2023.
- [5] S. Tonekaboni, D. Eytan, and A. Goldenberg, "Unsupervised representation learning for time series with temporal neighborhood coding," *arXiv preprint arXiv:2106.00750*, 2021.
- [6] E. Eldele, M. Ragab, Z. Chen, M. Wu, C. K. Kwok, X. Li, and C. Guan, "Time-series representation learning via temporal and contextual contrasting," *arXiv preprint arXiv:2106.14112*, 2021.
- [7] L. Yang and S. Hong, "Unsupervised time-series representation learning with iterative bilinear temporal-spectral fusion," in *International Conference on Machine Learning*. PMLR, 2022, pp. 25 038–25 054.
- [8] Z. Liang, J. Zhang, C. Liang, H. Wang, Z. Liang, and L. Pan, "Contrastive shapelet learning for unsupervised multivariate time series representation learning," *arXiv preprint arXiv:2305.18888*, 2023.
- [9] Z. Yue, Y. Wang, J. Duan, T. Yang, C. Huang, Y. Tong, and B. Xu, "Ts2vec: Towards universal representation of time series," in *Proceedings of the AAAI Conference on Artificial Intelligence*, vol. 36, no. 8, 2022, pp. 8980–8987.
- [10] G. Zerveas, S. Jayaraman, D. Patel, A. Bhamidipaty, and C. Eickhoff, "A transformer-based framework for multivariate time series representation learning," in *Proceedings of the 27th ACM SIGKDD conference on knowledge discovery & data mining*, 2021, pp. 2114–2124.
- [11] D. Zhu, D. Song, Y. Chen, C. Lumezanu, W. Cheng, B. Zong, J. Ni, T. Mizoguchi, T. Yang, and H. Chen, "Deep unsupervised binary coding networks for multivariate time series retrieval," in *Proceedings of the AAAI Conference on Artificial Intelligence*, vol. 34, no. 02, 2020, pp. 1403–1411.
- [12] A. Bagnall, H. A. Dau, J. Lines, M. Flynn, J. Large, A. Bostrom, P. Southam, and E. Keogh, "The uea multivariate time series classification archive, 2018," *arXiv preprint arXiv:1811.00075*, 2018.
- [13] W. Tang, L. Liu, and G. Long, "Interpretable time-series classification on few-shot samples," in *2020 International Joint Conference on Neural Networks (IJCNN)*. IEEE, 2020, pp. 1–8.
- [14] Z. Wang, T. Oates *et al.*, "Encoding time series as images for visual inspection and classification using tiled convolutional neural networks," in *Workshops at the twenty-ninth AAAI conference on artificial intelligence*, vol. 1. AAAI Menlo Park, CA, USA, 2015.
- [15] S.-H. Park, N. S. Syazwany, and S.-C. Lee, "Meta-feature fusion for few-shot time series classification," *IEEE Access*, 2023.
- [16] P. Schäfer and M. Höggqvist, "Sfa: a symbolic fourier approximation and index for similarity search in high dimensional datasets," in *Proceedings of the 15th international conference on extending database technology*, 2012, pp. 516–527.
- [17] S. Ren, Z. Gao, T. Hua, Z. Xue, Y. Tian, S. He, and H. Zhao, "Co-advise: Cross inductive bias distillation," in *Proceedings of the IEEE/CVF Conference on computer vision and pattern recognition*, 2022, pp. 16 773–16 782.
- [18] Q. Meng, H. Qian, Y. Liu, Y. Xu, Z. Shen, and L. Cui, "Unsupervised representation learning for time series: A review," *arXiv preprint arXiv:2308.01578*, 2023.
- [19] P. Vadiraja and M. A. Chattha, "A survey on knowledge integration techniques with artificial neural networks for seq-2-seq/time series models," *arXiv preprint arXiv:2008.05972*, 2020.
- [20] Q. Ma, J. Zheng, S. Li, and G. W. Cottrell, "Learning representations for time series clustering," *Advances in neural information processing systems*, vol. 32, 2019.
- [21] P. Malhotra, V. TV, L. Vig, P. Agarwal, and G. Shroff, "Timenet: Pre-trained deep recurrent neural network for time series classification," *arXiv preprint arXiv:1706.08838*, 2017.
- [22] H. Qian, T. Tian, and C. Miao, "What makes good contrastive learning on small-scale wearable-based tasks?" in *Proceedings of the 28th ACM SIGKDD Conference on Knowledge Discovery and Data Mining*, 2022, pp. 3761–3771.
- [23] T. Huynh, S. Kornblith, M. R. Walter, M. Maire, and M. Khademi, "Boosting contrastive self-supervised learning with false negative cancellation," in *Proceedings of the IEEE/CVF winter conference on applications of computer vision*, 2022, pp. 2785–2795.
- [24] T. Chen, S. Kornblith, M. Norouzi, and G. Hinton, "A simple framework for contrastive learning of visual representations," in *International conference on machine learning*. PMLR, 2020, pp. 1597–1607.
- [25] J.-B. Grill, F. Strub, F. Altché, C. Tallec, P. Richemond, E. Buchatskaya, C. Doersch, B. Avila Pires, Z. Guo, M. Gheshlaghi Azar *et al.*, "Bootstrap your own latent—a new approach to self-supervised learning," *Advances in neural information processing systems*, vol. 33, pp. 21 271–21 284, 2020.
- [26] I. Dave, R. Gupta, M. N. Rizve, and M. Shah, "Tclr: Temporal contrastive learning for video representation," *Computer Vision and Image Understanding*, vol. 219, p. 103406, 2022.
- [27] S. Ma, Z. Zeng, D. McDuff, and Y. Song, "Active contrastive learning of audio-visual video representations," *arXiv preprint arXiv:2009.09805*, 2020.
- [28] J.-Y. Franceschi, A. Dieuleveut, and M. Jaggi, "Unsupervised scalable representation learning for multivariate time series," *Advances in neural information processing systems*, vol. 32, 2019.
- [29] H. Wu, T. Hu, Y. Liu, H. Zhou, J. Wang, and M. Long, "Timesnet: Temporal 2d-variation modeling for general time series analysis," *arXiv preprint arXiv:2210.02186*, 2022.
- [30] T. Chen, S. Kornblith, K. Swersky, M. Norouzi, and G. E. Hinton, "Big self-supervised models are strong semi-supervised learners," *Advances in neural information processing systems*, vol. 33, pp. 22 243–22 255, 2020.
- [31] A. v. d. Oord, Y. Li, and O. Vinyals, "Representation learning with contrastive predictive coding," *arXiv preprint arXiv:1807.03748*, 2018.
- [32] J. Li, P. Zhou, C. Xiong, and S. C. Hoi, "Prototypical contrastive learning of unsupervised representations," *arXiv preprint arXiv:2005.04966*, 2020.
- [33] M. Caron, I. Misra, J. Mairal, P. Goyal, P. Bojanowski, and A. Joulin, "Unsupervised learning of visual features by contrasting cluster assignments," *Advances in neural information processing systems*, vol. 33, pp. 9912–9924, 2020.
- [34] Q. Meng, H. Qian, Y. Liu, L. Cui, Y. Xu, and Z. Shen, "Mhcl: Masked hierarchical cluster-wise contrastive learning for multivariate time series," in *Proceedings of the AAAI Conference on Artificial Intelligence*, vol. 37, no. 8, 2023, pp. 9153–9161.
- [35] A. Hyvarinen and H. Morioka, "Unsupervised feature extraction by time-contrastive learning and nonlinear ica," *Advances in neural information processing systems*, vol. 29, 2016.
- [36] S. Winograd, "On computing the discrete fourier transform," *Mathematics of computation*, vol. 32, no. 141, pp. 175–199, 1978.
- [37] A. Grossmann, R. Kronland-Martinet, and J. Morlet, "Reading and understanding continuous wavelet transforms," in *Wavelets: Time-Frequency Methods and Phase Space Proceedings of the International Conference, Marseille, France, December 14–18, 1987*. Springer, 1990, pp. 2–20.
- [38] A. Notaristefano, G. Chicco, and F. Pigliione, "Data size reduction with symbolic aggregate approximation for electrical load pattern grouping," *IET Generation, Transmission & Distribution*, vol. 7, no. 2, pp. 108–117, 2013.
- [39] R. Girdhar, A. El-Nouby, Z. Liu, M. Singh, K. V. Alwala, A. Joulin, and I. Misra, "Imagebind: One embedding space to bind them all," in *Proceedings of the IEEE/CVF Conference on Computer Vision and Pattern Recognition*, 2023, pp. 15 180–15 190.
- [40] G. Yariv, I. Gat, L. Wolf, Y. Adi, and I. Schwartz, "Audiotoken: Adaptation of text-conditioned diffusion models for audio-to-image generation," *arXiv preprint arXiv:2305.13050*, 2023.
- [41] A. Bardes, J. Ponce, and Y. LeCun, "Vicreg: Variance-invariance-covariance regularization for self-supervised learning," *arXiv preprint arXiv:2105.04906*, 2021.
- [42] R. Balestrieri and Y. LeCun, "Contrastive and non-contrastive self-supervised learning recover global and local spectral embedding methods," *Advances in Neural Information Processing Systems*, vol. 35, pp. 26 671–26 685, 2022.

- [43] A. Radford, J. W. Kim, C. Hallacy, A. Ramesh, G. Goh, S. Agarwal, G. Sastry, A. Askell, P. Mishkin, J. Clark *et al.*, "Learning transferable visual models from natural language supervision," in *International conference on machine learning*. PMLR, 2021, pp. 8748–8763.
- [44] L. Trevisan, "Lecture notes on graph partitioning, expanders and spectral methods," *University of California, Berkeley*, <https://people.eecs.berkeley.edu/luca/books/expanders-2016.pdf>, 2017.
- [45] Z. Li, Y. Zhao, J. Han, Y. Su, R. Jiao, X. Wen, and D. Pei, "Multivariate time series anomaly detection and interpretation using hierarchical inter-metric and temporal embedding," in *Proceedings of the 27th ACM SIGKDD conference on knowledge discovery & data mining*, 2021, pp. 3220–3230.
- [46] Y. Su, Y. Zhao, C. Niu, R. Liu, W. Sun, and D. Pei, "Robust anomaly detection for multivariate time series through stochastic recurrent neural network," in *Proceedings of the 25th ACM SIGKDD international conference on knowledge discovery & data mining*, 2019, pp. 2828–2837.
- [47] N. Zhang and S. Sun, "Multiview unsupervised shapelet learning for multivariate time series clustering," *IEEE Transactions on Pattern Analysis and Machine Intelligence*, vol. 45, no. 4, pp. 4981–4996, 2022.
- [48] K. Hundman, V. Constantinou, C. Laporte, I. Colwell, and T. Soderstrom, "Detecting spacecraft anomalies using lstms and nonparametric dynamic thresholding," in *Proceedings of the 24th ACM SIGKDD international conference on knowledge discovery & data mining*, 2018, pp. 387–395.
- [49] F. Karim, S. Majumdar, H. Darabi, and S. Harford, "Multivariate lstm-fns for time series classification," *Neural networks*, vol. 116, pp. 237–245, 2019.
- [50] X. Zhang, Y. Gao, J. Lin, and C.-T. Lu, "Tapnet: Multivariate time series classification with attentional prototypical network," in *Proceedings of the AAAI Conference on Artificial Intelligence*, vol. 34, no. 04, 2020, pp. 6845–6852.
- [51] G. Li, B. Choi, J. Xu, S. S. Bhowmick, K.-P. Chun, and G. L.-H. Wong, "Shapenet: A shapelet-neural network approach for multivariate time series classification," in *Proceedings of the AAAI conference on artificial intelligence*, vol. 35, no. 9, 2021, pp. 8375–8383.
- [52] W. Tang, G. Long, L. Liu, T. Zhou, M. Blumenstein, and J. Jiang, "Omni-scale cnns: a simple and effective kernel size configuration for time series classification," *arXiv preprint arXiv:2002.10061*, 2020.
- [53] Q. Xiao, B. Wu, Y. Zhang, S. Liu, M. Pechenizkiy, E. Mocanu, and D. C. Mocanu, "Dynamic sparse network for time series classification: Learning what to "see"," *Advances in Neural Information Processing Systems*, vol. 35, pp. 16 849–16 862, 2022.
- [54] J. Lines, S. Taylor, and A. Bagnall, "Time series classification with hivecote: The hierarchical vote collective of transformation-based ensembles," *ACM Transactions on Knowledge Discovery from Data (TKDD)*, vol. 12, no. 5, pp. 1–35, 2018.
- [55] H. Li, "Multivariate time series clustering based on common principal component analysis," *Neurocomputing*, vol. 349, pp. 239–247, 2019.
- [56] K. Ø. Mikalsen, F. M. Bianchi, C. Soguero-Ruiz, and R. Jenssen, "Time series cluster kernel for learning similarities between multivariate time series with missing data," *Pattern Recognition*, vol. 76, pp. 569–581, 2018.
- [57] M. Ozer, A. Sapienza, A. Abeliuk, G. Muric, and E. Ferrara, "Discovering patterns of online popularity from time series," *Expert Systems with Applications*, vol. 151, p. 113337, 2020.
- [58] D. Ienco and R. Interdonato, "Deep multivariate time series embedding clustering via attentive-gated autoencoder," in *Advances in Knowledge Discovery and Data Mining: 24th Pacific-Asia Conference, PAKDD 2020, Singapore, May 11–14, 2020, Proceedings, Part I 24*. Springer, 2020, pp. 318–329.
- [59] Q. Zhang, J. Wu, P. Zhang, G. Long, and C. Zhang, "Salient subsequence learning for time series clustering," *IEEE transactions on pattern analysis and machine intelligence*, vol. 41, no. 9, pp. 2193–2207, 2018.
- [60] A. A. Inc. (2019) tsaug: An open-source package for time series data augmentation. [Online]. Available: <https://tsaug.readthedocs.io/en/stable/references.html>